A Structure−Function Study of a Proton Transport Pathway in the γ-Class Carbonic Anhydrase from *Methanosarcina thermophila*†

Brian C. Tripp and James G. Ferry*

Department of Biochemistry and Molecular Biology, Eberly College of Science, The Pennsylvania State University, University Park, Pennsylvania 16802-4500

Received January 31, 2000; Revised Manuscript Received May 17, 2000

ABSTRACT: Four glutamate residues in the prototypic γ-class carbonic anhydrase from *Methanosarcina thermophila* (Cam) were characterized by site-directed mutagenesis and chemical rescue studies. Alanine substitution indicated that an external loop residue, Glu 84, and an internal active site residue, Glu 62, are both important for CO_2 hydration activity. Two other external loop residues, Glu 88 and Glu 89, are less important for enzyme function. The two E84D and -H variants exhibited significant activity relative to wild-type activity in pH 7.5 MOPS buffer, suggesting that the original glutamate residue could be substituted with other ionizable residues with similar pK_a values. The E84A, -C, -K, -Q, -S, and -Y variants exhibited large decreases in k_{cat} values in pH 7.5 MOPS buffer, but only exhibited small changes in k_{cat}/K_m. These same six variants were all chemically rescued by pH 7.5 imidazole buffer, with 23−46-fold increases in the apparent k_{cat}. These results are consistent with Glu 84 functioning as a proton shuttle residue. The E62D variant exhibited a 3-fold decrease in k_{cat} and a 2-fold decrease in k_{cat}/K_m relative to those of the wild type in pH 7.5 MOPS buffer, while other substitutions (E62A, -C, -H, -Q, -T, and -Y) resulted in much larger decreases in both k_{cat} and k_{cat}/K_m. Imidazole did not significantly increase the k_{cat} values and slightly decreased the k_{cat}/K_m values of most of the Glu 62 variants. These results indicate a primary preference for a carboxylate group at position 62, and support a proposed catalytic role for residue Glu 62 in the CO_2 hydration step, but do not definitively establish its role in the proton transport step.

There are three independently evolved classes of carbonic anhydrases (α, β, and γ) that catalyze the reversible hydration of CO_2 (eq 1) (*1*). The α-class is the best characterized for which a two-step zinc hydroxide mechanism has been proposed.

$$CO_2 + H_2O \rightleftharpoons H^+ + HCO_3^- \quad (1)$$

The first step is the nucleophilic attack of a zinc-bound hydroxide ion on the weakly bound CO_2 (eq 2). The second step is the regeneration of the active site by the ionization of zinc-bound water molecule into a proton, which must be removed from the active site, and a zinc-bound hydroxide ion (eq 3). The zinc ion acts as a Lewis acid to lower the pK_a of the water from 14 to approximately 7.

$$Zn^{2+}\text{-}OH^- + CO_2 \rightleftharpoons Zn^{2+} + HCO_3^- \quad (2)$$

$$Zn^{2+} + H_2O \rightleftharpoons Zn^{2+}\text{-}OH^- + H^+ \quad (3)$$

Carbonic anhydrases with slower CO_2 hydration rates ($k_{cat} \leq 10^4$ s^{-1}) transfer the proton directly to buffer or water molecules in solution (eq 3), as this is the fastest rate at which protons can transfer from an acidic group with a pK_a of 7 to water (*2*). Faster carbonic anhydrase enzymes, such as α-class mammalian carbonic anhydrase II, exhibit k_{cat} values in the range of 10^4-10^6 s^{-1}, and must transfer the proton from the zinc-bound water molecule to an intermediate PSR[1] as shown in eq 3a, and then to an external buffer molecule (B) (eq 3b).

$$PSR + Zn^{2+}\text{−}H_2O \rightleftharpoons Zn^{2+}\text{-}OH^- + PSR\text{-}H^+ \quad (3a)$$

$$PSR\text{-}H^+ + B \rightleftharpoons PSR + B\text{-}H^+ \quad (3b)$$

The study of PSRs has been restricted to the α-class enzymes which utilize ionizable residues histidine, glutamate, aspartate, and lysine, with intrinsic pK_a values in the range of 4−10 which can shuttle protons from the zinc-bound water molecule (Zn-H_2O) to buffer (B) (*3*−*15*). Proton transfers from the zinc-bound water molecule to the PSR and possibly from the PSR to the external buffer are thought to occur through networks of hydrogen-bonded water molecules ("proton wires"), rather than by direct transfer from the zinc-bound water to the PSR (*7*, *16*−*21*). In the fast α-class carbonic anhydrase II, under conditions of high buffer concentration the rate-limiting step in the forward direction

† This work was supported by a grant from the National Institutes of Health to J.G.F. (GM44661). B.C.T. is supported by a National Science Foundation-Research Training Grant Fellowship (DBI-9602232).

* Corresponding author. Phone: (814) 863-5721. Fax: (814) 863-6217. E-mail: jgf3@psu.edu.

[1] Abbreviations: PSR, proton shuttle residue; Cam, *M. thermophila* carbonic anhydrase produced in *Escherichia coli*; SHIE, solvent hydrogen isotope effect; MES, 2-(*N*-morpholino)ethanesulfonic acid; MOPS, 2-(*N*-morpholino)propanesulfonic acid; TAPS, *N*-tris(hydroxymethyl)methyl-3-aminopropanesulfonic acid; CHES, 2-(*N*-cyclohexylamino)ethanesulfonic acid.

10.1021/bi0001877 CCC: $19.00
Published on Web 07/12/2000

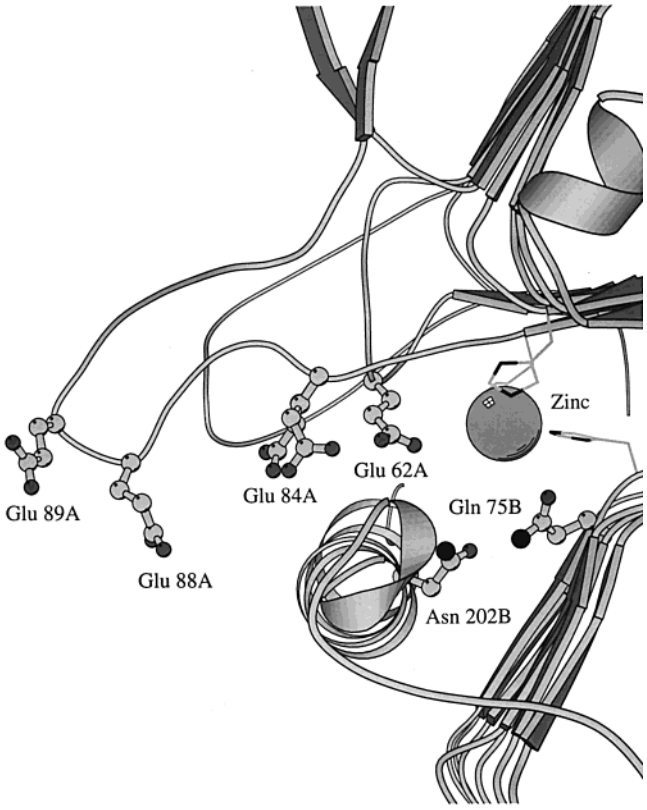

FIGURE 1: View of Cam active site and external loop acidic residues. Two distinct conformations are shown for Glu 84. Distances in angstroms between the zinc ion and the α-carbon and nearest oxygen atoms (respectively) for the four residues are as follows: Glu 62, 7.5 and 4.5; Glu 84, 8.6 and 8.0; Glu 88, 17.0 and 16.3; and Glu 89, 20.3 and 21.5. This image was prepared with the Molscript software package version 2.1 [Kraulis, P. J. (1991) *J. Appl. Crystallogr. 24*, 946−950].

is generally thought to be the removal of the proton from the active site (eq 3) (*1*, *22*). This implies that the turnover number (k_{cat}) is a reflection of the rate of proton transport (eq 3), while the catalytic efficiency (k_{cat}/K_m) is more reflective of the CO_2 hydration step (eq 2), and is generally insensitive to the rate of proton transport. The β-class carbonic anhydrase appears to follow the same zinc hydroxide mechanism proposed for the α-class carbonic anhydrases (*23*); however, only one study has been reported on the steps involved in proton transfer (*24*).

The carbonic anhydrase from the thermophilic methanoarchaeon *Methanosarcina thermophila*, Cam, is the prototype of the γ-class and the only γ-carbonic anhydrase that has been characterized. Cam has several features that differentiate it from the other two enzyme classes. The protein fold is composed of a left-handed β-helix motif, interrupted by three protruding loops and followed by short and long α-helix structures (*25*). The Cam monomer self-associates into a homotrimer structure with an approximate molecular mass of 70 kDa. The Cam active site contains three histidine residues that coordinate a zinc ion with a geometry very similar to that found in the α-class. However, the similarities between the active site of Cam and the α-class end there. Unlike the monomeric α-class carbonic anhydrases, the Cam active sites are located at the interface between pairs of monomers, with residues in the active site donated from both monomer faces (Figure 1). Two of the metal binding residues are donated by monomer A (His 81-A and His 122-A), and the third is from adjacent monomer B (His 117-B). Other residues in the active site of Cam are also donated from both monomer faces and bear little resemblance to residues in the active site of the well-characterized α-class carbonic anhydrases for which specific functions have been assigned (*1*).

Although the active site residues are unlike the α-class, the proposed kinetic mechanism for Cam involves the same two-step mechanism, with intramolecular proton transfer as the rate-limiting step under high buffer concentrations (*26*). Cam is also a relatively fast carbonic anhydrase, with k_{cat} values approaching 10^5 s^{-1} (*26*), implying the presence of a PSR. There is no equivalent α-class His 64 PSR in the Cam active site, leaving open the question of the mechanism of proton transfer, and the identity of any possible PSRs. Analysis of high-resolution structures for Cam and Cam complexed with bicarbonate has led to a proposal in which residue Glu 62 is involved in the CO_2 hydration step of catalysis (eq 2) and is also potentially involved in proton transfer (eq 3) along with residue Glu 84 (*27*). Here, we report site-directed mutagenesis results from investigations of the role of residues Glu 62 and Glu 84 and other potential PSRs in Cam.

MATERIALS AND METHODS

Mutagenesis and Expression. A plasmid encoding the sequence of a putative mature or soluble form of Cam, termed pBA1416NB, derived from plasmid pT7-7, was used as the starting plasmid for all site-directed mutagenesis experiments (*28*). This form of Cam has a 34-amino acid deletion from the N-terminal sequence, which has properties characteristic of a secretory signal peptide leader sequence. Unique *Ban*II and *Bsr*GI restriction sites were introduced into this plasmid using the QuikChange site-directed mutagenesis kit (Stratagene, La Jolla, CA), to allow cassette mutagenesis of a region encoding residues 76−90. Other single mutations were introduced at various positions by using the same kit. Mutations were confirmed by DNA sequencing of the plasmids. *Escherichia coli* strain BL21(DE3) or BL21(DE3) Gold was transformed with pBA1416NA or derivative-mutated plasmids, and used to inoculate Luria-Bertani broth containing 100 μg/mL ampicillin and 500 μM $ZnSO_4$. Cells were grown at 37 °C to an A_{600} of 0.4−0.8, and induced to overproduce Cam variants by addition of isopropyl thiogalactopyranoside (IPTG) to a final concentration of 0.8 mM, followed by continued growth at 37 °C for 3 h. Cells were then harvested by centrifugation and stored frozen at −80 °C until lysis was performed. Molecular biology procedures were performed according to Sambrook et al. (*29*).

Purification. Cells were lysed by resuspension in 50 mM MOPS buffer to an A_{600} of 2−10, followed by two passes through a chilled French press at a pressure of 1000 lb/in.^{2} (1 lb/in.^{2} = 6.9 kPa). Cell lysate was centrifuged at 20000−50000*g* for 20 min, followed by sterile filtration of the supernatant through a 0.45 μm filter. The soluble cell extract solution was then loaded onto a Q Sepharose Fast Flow column (Amersham Pharmacia Biotech, Piscataway, NJ) and washed with several column volumes of pH 7.5, 50 mM MOPS buffer. A gradient of 0 to 1.0 M NaCl was then applied over 10 bed volumes to the column to elute the Cam

fractions, which typically eluted at a NaCl concentration of 0.5 M. The Cam fractions were then pooled and diluted 2-fold with 3.0 M $(NH_4)_2SO_4$ previously equilibrated with Chelex resin (Bio-Rad, Hercules, CA) to remove the contaminating iron, to give a final $(NH_4)_2SO_4$ concentration of 1.5 M. This solution was then loaded onto a Phenyl Sepharose high-performance column (Amersham Pharmacia Biotech) previously equilibrated with pH 7.5, 50 mM MOPS, 1.5 M $(NH_4)_2SO_4$ buffer. The column was washed with several bed volumes of equilibration buffer, and then the Cam protein was eluted by applying a decreasing gradient of 1.5 to 0 M $(NH_4)_2SO_4$ buffer. Cam fractions were then pooled, dialyzed against 50 mM, pH 7.5 MOPS buffer, aliquoted, and frozen in liquid nitrogen, and stored at −80 °C until they were used further.

Gel Filtration Chromatography. A Superose 12 high-resolution gel filtration column (Amersham Pharmacia Biotech) was equilibrated with pH 7.5, 50 mM MOPS, 50 mM Na_2SO_4 buffer. Each Cam variant (200 μL) at a concentration of 50 μM was injected onto the column and eluted from the column using a buffer flow rate of 0.5 mL/min. The eluting protein was detected by measuring the UV absorbance at a wavelength of 280 nm.

Steady-State Kinetic Measurements. Wild-type Cam and variants of interest were assayed for carbonic anhydrase activity by the method of Khalifah (*30*), using a model SF-2001 KinTek stopped-flow instrument (KinTek Corp., Austin, TX). Enzyme monomer concentrations ranged from 200 nM to 15 μM, and were determined by measuring A_{280}s of protein solutions, using a theoretical molar absorbance value of 15 990 M^{-1} cm^{-1}, with a computed monomer molecular mass of 22 873 Da. Buffer−indicator dye pairs used were MES and chlorophenol red (at pH 5.7−6.9) measured at a wavelength of 574 nm, imidazole, 1-methylimidazole, 1,2-dimethylimidazole, or MOPS and 4-nitrophenol (at pH 6.5−7.7) measured at a wavelength of 400 nm, TAPS and *m*-cresol purple (at pH 7.7−9.1) measured at a wavelength of 578 nm, and CHES and thymol blue (at pH 8.9−9.5) measured at a wavelength of 590 nm. Unless otherwise noted, buffer concentrations were 50 mM and the total ionic strength was adjusted to 0.2 M with Na_2SO_4. Acetate and pyrazole rescue experiments were performed using 50 mM sodium acetate or 50 mM pyrazole, in addition to pH 7.5, 50 mM MOPS. Final pH indicator concentrations ranged from 2.0×10^{-6} to 1.0×10^{-4} M. Saturated solutions of CO_2 (32.9 mM in H_2O, 38.1 mM in D_2O) were prepared by bubbling CO_2 gas into deionized water or D_2O at 25 °C. The experimental CO_2 concentrations were varied from 4.7 to 24 mM. Only the initial 5−10% of the pre-steady-state kinetic data was used for kinetic analysis, using the average of 6−10 reaction traces per experiment. The initial rate data were fit to the Michaelis−Menten equation to obtain experimental values for k_{cat} and K_m. The pH-independent values of k_{cat} and pK_a for CO_2 hydration were determined by fitting the experimental pH-dependent Michaelis−Menten parameter k_{cat} to eq 4.

$$k_{cat}^{obs} = k_{cat}(1 + 10^{pK_a - pH}) \quad (4)$$

The pH-independent values for k_{cat}/K_m, k_{cat}/K_m^{II}, pK_a^I, and pK_a^{II} for CO_2 hydration of the wild type and the E84H variant were determined by fitting the pH-dependent Michaelis−Menten parameter k_{cat}/K_m to eq 5.

$$k_{cat}/K_m^{obs} = [(k_{cat}/K_m) \times 10^{pK_a^{II} - pH} + k_{cat}/K_m^{II}]/ (1 + 10^{pK_a^{II} + pK_a^{I} - 2pH} + 10^{pK_a^{I} - pH} + 10^{pK_a^{II} - pH}) \quad (5)$$

Solvent hydrogen isotope effect (SHIE) studies were performed in pD 6.5, 50 mM MES; pD 7.5, 50 mM MOPS; and pD 8.5, 50 mM TAPS buffers, with the ionic strength adjusted to 0.2 M with Na_2SO_4, at a temperature of 25 °C, using solutions with final D_2O concentrations of >95%. All pD values are uncorrected pH electrode readings. The CO_2 concentrations were varied from 5.4 to 27 mM, based on saturating solutions of D_2O at 25 °C. All data fits were performed with the Kaleidagraph software package (Synergy Software, Reading, PA).

Electrostatic Surface Potential. The GRASP software package (*31*) running on a Silicon Graphics UNIX workstation was used to compute the electrostatic surface potential of Cam, using the X-ray structure coordinate file for Cam, 1THJ (*25*), available from the Protein Data Bank. Electrostatic parameters that were used included an ionic radius of 2.0 Å, an external solvent dielectric of 80, an internal dielectric of 2.0, and a salt concentration of 0.2 M.

RESULTS

Generation and Initial Characterization of Cam Variants. The surface electrostatic potential of Cam (data not shown) reveals a loop region (residues 83−90) containing residues Glu 89, Glu 88, and Glu 84 which form an acidic "valley" extending from the bulk solvent to residue Glu 62 which is adjacent to the active site zinc (Figure 1). The arrangement of these four glutamates suggests a potential role in proton transfer from the zinc-bound water molecule to buffer in the bulk solvent. PSR roles for Glu 62 and Glu 84 have also been proposed on the basis of high-resolution crystal structures of Cam and Cam complexed with bicarbonate (*27*). Thus, each of the four glutamates was replaced by site-directed mutagenesis (Table 1) to determine its role in catalysis. All Cam variants were produced in the soluble fraction of *E. coli*, with yields similar to that of the wild type (25−50 mg/L of culture). Gel filtration chromatography indicated that all variants were trimers in accord with the wild type (*28*). These results indicate that replacement of Glu 89, Glu 88, Glu 84, and Glu 62 with any of the residues listed in Table 1 does not result in gross conformational changes in the protein structure. All Cam variants exhibited normal Michaelis−Menten kinetics.

pH-Dependent Solvent Hydrogen Isotope Effects with Wild-Type Cam. The previously reported SHIE on the k_{cat} value of Cam at saturating buffer concentrations showed that intramolecular proton transfer is rate-limiting at pH 8.5 (*26*). These studies were extended to pH 7.5 and 6.5 as a prerequisite for interpretation of CO_2 hydration activities of the wild type and replacement variants in imidazole or MOPS buffer. The SHIE for catalysis in the CO_2 hydration reaction was measured using a concentration of 50 mM MES (pH/D 6.5), MOPS (pH/D 7.5), or TAPS (pH/D 8.5) where intermolecular proton transfer to buffer is not rate-limiting. The ratio of $k_{cat}(H_2O)/k_{cat}(D_2O)$ was greater than 2.0 (Table 2) for the k_{cat} values at all three pH/D values, indicating that intramolecular proton transport is rate-limiting over the pH

Table 1: Michaelis−Menten Steady-State Kinetic Parameters for Wild-Type Cam and Variants with Substitutions at Glutamate 62, Glutamate 84, Glutamate 88, and Glutamate 89[a]

variant	buffer	k_{cat} ($\times 10^{-3}$ s^{-1})	K_m ($\times 10^{3}$ M)	k_{cat}/K_m ($\times 10^{-6}$ M^{-1} s^{-1})
wild-type	MOPS[b]	56.8 ± 5.8	27.8 ± 4.5	2.05 ± 0.54
	IMID[c]	71.9 ± 14.9	44.1 ± 12.5	1.63 ± 0.80
	MOPS-Ac[d]	24.7 ± 2.4	22.5 ± 3.8	1.09 ± 0.29
E62A	MOPS	0.72 ± 0.03	6.5 ± 0.7	0.11 ± 0.02
	IMID	1.07 ± 0.03	9.4 ± 0.7	0.11 ± 0.01
	MOPS-Ac	0.34 ± 0.01	5.5 ± 0.6	0.063 ± 0.009
E62C	MOPS	0.91 ± 0.03	3.8 ± 0.5	0.24 ± 0.04
E62D	MOPS	16.8 ± 0.3	18.8 ± 0.6	0.89 ± 0.04
E62H	MOPS	1.05 ± 0.07	7.6 ± 1.3	0.14 ± 0.03
E62Q	MOPS	0.41 ± 0.01	1.4 ± 0.3	0.29 ± 0.06
E62T	MOPS	0.86 ± 0.02	2.5 ± 0.4	0.35 ± 0.07
E62Y	MOPS	0.047 ± 0.004	3.0 ± 1.3	0.016 ± 0.008
E84A	MOPS	0.87 ± 0.02	1.5 ± 0.2	0.58 ± 0.11
	IMID	35.1 ± 1.5	8.8 ± 1.0	4.00 ± 0.60
	MOPS-Ac	0.80 ± 0.013	0.8 ± 0.2	1.02 ± 0.24
E84C	MOPS	0.72 ± 0.02	1.1 ± 0.3	0.68 ± 0.18
E84D	MOPS	21.0 ± 0.5	18.1 ± 0.8	1.14 ± 0.08
E84H	MOPS	9.5 ± 0.2	3.2 ± 0.3	3.00 ± 0.28
E84K	MOPS	1.9 ± 0.04	1.5 ± 0.3	1.24 ± 0.26
E84Q	MOPS	1.3 ± 0.03	1.2 ± 0.3	1.12 ± 0.29
E84S	MOPS	1.08 ± 0.03	2.1 ± 0.4	0.51 ± 0.11
E84Y	MOPS	0.51 ± 0.02	2.1 ± 0.4	0.25 ± 0.06
E88A	MOPS	26.5 ± 2.5	16.9 ± 3.0	1.57 ± 0.43
E89A	MOPS	29.1 ± 2.0	19.3 ± 2.4	1.51 ± 0.29
E62A/E84A	MOPS	0.21 ± 0.01	2.9 ± 0.8	0.073 ± 0.024
E62D/E84D	MOPS	4.7 ± 0.2	5.4 ± 1.0	0.87 ± 0.20

[a] The initial pH of all assay buffers was 7.5; the ionic strength of each solution was adjusted to 0.2 M with Na_2SO_4. [b] MOPS, 50 mM MOPS. [c] IMID, 50 mM imidazole. [d] MOPS-Ac, 50 mM MOPS and 50 mM sodium acetate.

range. A moderate SHIE was also observed for the k_{cat}/K_m value of wild-type Cam at all three pH/D values (Table 2).

Kinetic Analysis of E62A, E84A, E88A, and E89A Variants. The k_{cat} values for the E62A and E84A variants in pH 7.5 MOPS buffer were similar (1.3 and 1.5% of the wild-type value), whereas the k_{cat}/K_m values were significantly different (5.4 and 28% of the wild-type value) (Table 1). These results indicate that residues Glu 62 and Glu 84 are important for catalysis. However, the 5-fold difference in k_{cat}/K_m observed for these two variants in MOPS buffer suggests that the functions for these two glutamates are nonequivalent. The k_{cat} values for the E88A and E89A variants were 47 and 51% of the wild-type k_{cat} in pH 7.5 MOPS buffer, whereas the k_{cat}/K_m values were not significantly different from the wild-type value. These results indicate that Glu 88 and Glu 89 are of only minor importance in catalysis.

The ability of imidazole to rescue the k_{cat} of α-class carbonic anhydrase replacement variants is considered strong evidence of rate-limiting proton transfer and is evidence for involvement of the substituted residue in the proton transfer step of catalysis (*3*). Thus, k_{cat} values for wild-type Cam and all variants were determined in the presence of imidazole buffer and the much larger MOPS buffer at pH 7.5. The wild-type enzyme exhibited a 1.3-fold increase in k_{cat} when imidazole replaced MOPS (pH 7.5) (Table 1). As proton transport is rate-limiting at pH 7.5, this result is consistent with imidazole entering the active site and enhancing the rate of proton transfer. A time course for catalysis by the E84A variant and wild-type Cam in the presence of 50 mM MOPS or imidazole buffers is shown in Figure 2. In contrast to that of the wild type, the k_{cat} for the E84A variant was 40-fold greater in imidazole than in MOPS buffer (Table 1), although the kinetic rate was not measured under saturating imidazole concentrations. Similar results were obtained with 1-methylimidazole and 1,2-dimethylimidazole (Supporting Information). The wild-type k_{cat} was nearly independent of imidazole concentrations of >20 mM (Figure 3). In contrast, the E84A variant exhibited a large dependence of k_{cat} on imidazole concentration, with increasing k_{cat} values approaching a maximum at 200 mM (Figure 3). The k_{cat}/K_m values for both the wild type and the E84A variant decreased with increasing imidazole concentrations of ≥20 mM (Figure 3). The k_{cat} values of the E62A, E88A, and E89A variants in imidazole buffer were less than 2-fold greater than in MOPS (Table 1, Supporting Information), results similar to that obtained for the wild type. Pyrazole, with a low pK_a of 2.5, also did not rescue either of the E62A or E84A variants (Supporting Information), despite its small size and structural similarity to imidazole. This result demonstrates that imidazole did not increase k_{cat} by a reversal of structural changes imposed by any of the replacements. Acetate, which mimics the deleted side chain of E84A and E62A variants, did not rescue the k_{cat} value of either variant (Table 1), with a 10% decrease in k_{cat} for the E84A variant and a 50% decrease in the k_{cat} values of the wild type and the E62A variant (Table 1).

Kinetic Analysis of E62C, -D, -H, -Q, -T, and -Y Variants. Additional Cam variants were generated by site-directed replacement to further probe the roles of Glu 62 and Glu 84 in catalysis. The E62D variant had significant k_{cat} (30% of the wild-type value) and k_{cat}/K_m (43% of the wild-type value) values in pH 7.5, 50 mM MOPS buffer (Table 1). The other E62C, -H, -Q, -T, and -Y variants had k_{cat} values in MOPS buffer that were less than 2% of the wild-type value and k_{cat}/K_m values in the range of 1−17% of the wild-type value with a mean k_{cat}/K_m value of 10% of the wild-type value (Table 1). Substitution of Glu 62 with cysteine, glutamine, and threonine produced variants with significant k_{cat}/K_m values relative to the wild-type value (12, 14, and 17%, respectively), whereas substitution with histidine and tyrosine produced variants with lower k_{cat}/K_m values similar to results obtained with the E62A variant. As observed for the E62A variant, imidazole did not significantly rescue the k_{cat} values of the E62C, -D, -H, -Q, -T, and -Y variants. There was a slight decrease in k_{cat} and k_{cat}/K_m observed for the E62D variant upon replacement of MOPS buffer with imidazole (Supporting Information).

Kinetic Analysis of E84C, -D, -H, -K, -Q, -S, and -Y Variants. Replacement of Glu 84 with aspartate or histidine yielded variants with k_{cat} values that were 36 and 17% of the wild-type value in pH 7.5 MOPS buffer (Table 1), whereas the k_{cat} values of the E84C, -K, -Q, -S, and -Y variants were only 1−3% of the wild-type value, similar to results obtained with the E84A variant (Table 1, Supporting Information). The k_{cat}/K_m values of the E84C, -K, -Q, -S, and -Y variants in MOPS buffer ranged from 12 to 61% of the wild-type value with a mean k_{cat}/K_m of 37% of the wild-type value, like E84A. Thus, k_{cat} for the E84C, -K, -Q, -S, and -Y variants changed several-fold more than k_{cat}/K_m. The k_{cat}/K_m values of the E84D and -H variants with higher k_{cat} values were also within 2-fold of the wild-type value. The E84D and -H variants exhibited an only 1.7−2.3-fold

Table 2: pH-Dependent Solvent Hydrogen Isotope Steady-State Kinetic Data for Wild-Type Cam[a]

pH/D	$k_{cat}(H_2O)$ ($\times 10^{-3}$ s^{-1})	$k_{cat}(D_2O)$ ($\times 10^{-3}$ s^{-1})	$K_m(H_2O)$ ($\times 10^3$ M)	$K_m(D_2O)$ ($\times 10^3$ M)	$k_{cat}/K_m(H_2O)$ ($\times 10^{-6}$ M^{-1} s^{-1})	$k_{cat}/K_m(D_2O)$ ($\times 10^{-6}$ M^{-1} s^{-1})	$k_{cat}(H_2O)/k_{cat}(D_2O)$	$[k_{cat}/K_m(H_2O)]/[k_{cat}/K_m(D_2O)]$
6.5	18.6 ± 1.9	9.3 ± 0.10	28.5 ± 4.5	23.8 ± 4.6	0.65 ± 0.17	0.39 ± 0.08	2.0 ± 0.2	1.7 ± 0.8
7.5	56.8 ± 5.8	16.7 ± 0.09	27.8 ± 4.5	14.7 ± 1.7	2.04 ± 0.54	1.14 ± 0.14	3.4 ± 0.4	1.8 ± 0.7
8.5	58.9 ± 7.3	22.6 ± 0.19	20.0 ± 4.5	12.6 ± 2.4	2.94 ± 1.02	1.79 ± 0.36	2.6 ± 0.3	1.6 ± 0.9

[a] Assay buffers were made with 50 mM MES, 50 mM MOPS, or 50 mM TAPS, and the ionic strength of each solution was adjusted to 0.2 M with Na_2SO_4.

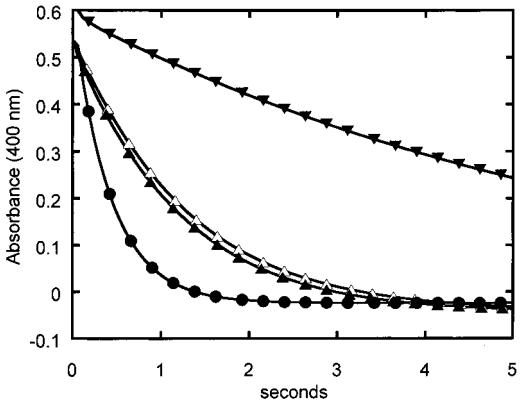

FIGURE 2: Plot of initial stopped-flow kinetic data for wild-type Cam and the E84A variant in MOPS and imidazole buffer. Experimental assay conditions are described in Materials and Methods: (▼) E84A variant in 50 mM MOPS, (●) E84A variant in 50 mM imidazole, (△) wild type in 50 mM MOPS, and (▲) wild type in 50 mM imidazole. The decrease in the absorbance of a pH indicator (*p*-nitrophenol) in solution reflects a decrease in pH due to generation of H^+ and HCO_3^- from CO_2.

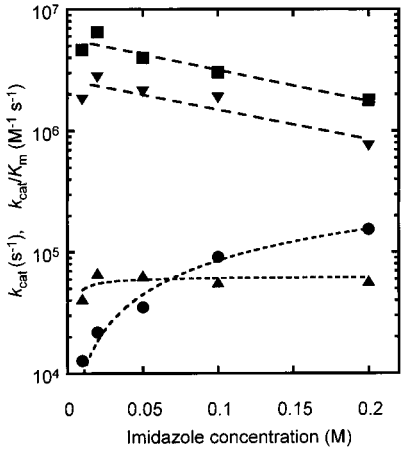

FIGURE 3: Plot of imidazole concentration dependence of steady-state kinetic parameters for wild-type Cam and the E84A variant: (▲) wild-type k_{cat} value, (▼) wild-type k_{cat}/K_m value, (●) E84A k_{cat} value, and (■) E84A k_{cat}/K_m value. The experimental assay conditions were as follows: temperature of 25 °C, total ionic strength adjusted to 0.2 M with Na_2SO_4, with pH 7.5 imidazole, and concentration varied from 10 to 200 mM.

increase in k_{cat} when imidazole buffer was substituted for MOPS (Supporting Information), a result similar to that obtained for the wild type, although these values were not obtained with saturating imidazole concentrations. In contrast, all other Glu 84 variants with much lower k_{cat} values relative to that of the wild type (E84C, -K, -Q, -S, and -Y) were rescued 23−46-fold in k_{cat} by replacing MOPS buffer with imidazole (Table 2, Supporting Information). These results are similar to those obtained for the E84A variant with a low k_{cat} value relative to that of the wild type.

Table 3: pH-Independent Michaelis−Menten Kinetic Parameters Derived from the pH Dependence of CO_2 Hydration Catalyzed by the Wild Type and E84H Cam Variants from *M. thermophila*[a]

	wild-type	E84H
k_{cat} ($\times 10^{-4}$ s^{-1})	7.1 ± 0.6	ND
pK_a (k_{cat})	6.9	ND
pK_a^I (k_{cat}/K_m^I)	6.5 ± 0.3	6.6 ± 0.2
pK_a^{II} (k_{cat}/K_m^{II})	8.5 ± 0.4	9.7 ± 0.6
k_{cat}/K_m^I ($\times 10^{-6}$ M^{-1} s^{-1})	1.7 ± 0.4	2.5 ± 0.3
k_{cat}/K_m^{II} ($\times 10^{-6}$ M^{-1} s^{-1})	3.9 ± 0.4	11.3 ± 8.1

[a] pH-independent kinetic parameters and pK_a values for CO_2 hydration were determined by fitting pH-dependent k_{cat} and k_{cat}/K_m data obtained over the pH range of 5.7−9.5 to eqs 4 and 5, as described in Materials and Methods.

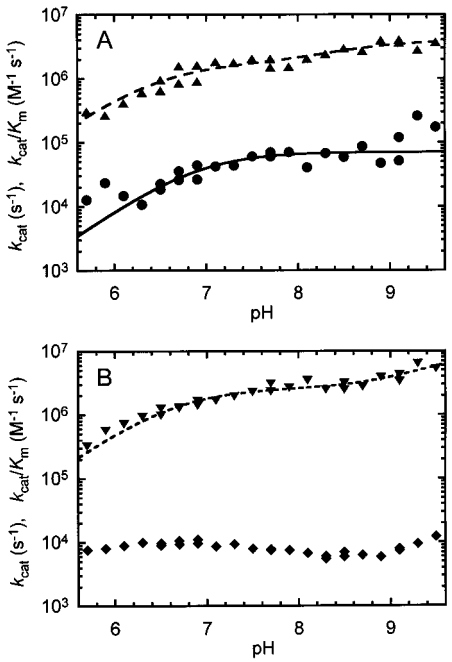

FIGURE 4: pH-dependent steady-state kinetic parameters for wild-type Cam and the E84H variant: (A) wild-type k_{cat} (●) and k_{cat}/K_m (▲) and (B) E84H k_{cat} (◆) and E84H k_{cat}/K_m (▼).

Different pH-dependent k_{cat} behaviors for the E84H variant and wild type might be expected if Glu 84 is a PSR and histidine is able to replace this function. The E84H variant exhibited enough residual activity so it could be reliably assayed over a broad pH range. The fit of the wild-type k_{cat}/K_m versus pH profile to a two-ionization model (eq 5) yielded pK_a values of 6.5 (pK_a^I) and 8.5 (pK_a^{II}) (Table 3), similar to previously reported results (*26*). The fit of the E84H variant k_{cat}/K_m versus pH data (Figure 4) to this model yielded pK_a values of 6.6 (pK_a^I) and 9.7 (pK_a^{II}). The presence of two pK_a values is similar to the wild-type case, although the higher value for pK_a^{II} is unexplained. A fit of the pH-dependent k_{cat} profile to a single-ionization model (eq 4)

indicated a pK_a of 6.9 for the wild type (Table 3), similar to the previously reported pK_a value of 6.8 (*26*). This model, however, could not satisfactorily fit the pH-dependent k_{cat} profile for the E84H variant. In contrast to the wild type, the E84H variant exhibited only a slight dependence of k_{cat} on pH (Figure 4).

Analysis of the E62A/E84A and E62D/E84D Double Variants. The double variants E62A/E84A and E62D/E84D were generated to investigate the possibility that Glu 62 and Glu 84 interact during catalysis of CO_2. The k_{cat} value of the E62A/E84A double variant in MOPS buffer was only 0.4% of the wild-type value (Table 1) and was only increased to 0.7% of the wild-type k_{cat} value in imidazole buffer (Supporting Information), a result similar to that observed for the E62A variant. The k_{cat}/K_m values of the E62A/E84A double variant were also very low, 3.6 and 4.7% of the wild-type k_{cat}/K_m value in MOPS and imidazole buffer, respectively (Table 1, Supporting Information).

The k_{cat} value of the E62D/E84D double substitution variant was only 8.3% of the wild-type value in MOPS buffer (Table 1), compared with 30% of the wild-type k_{cat} value observed for the E62D variant (Table 1) and 37% of the wild-type k_{cat} value observed for the E84D variant (Table 1). This greater decrease in k_{cat} of the double variant versus either of the single variants was further analyzed thermodynamically (*32*). The change in Gibbs free energy for catalysis by the E62D, E84D, and E62D/E84D variants relative to that of the wild type in MOPS buffer was computed from their respective k_{cat} values by applying the equation $\Delta G = RT \ln(k_{cat-wild-type}/k_{cat-variant})$. The E62D variant yielded a ΔG_1 value of 0.72 ± 0.33 kcal/mol; the E84D variant yielded a ΔG_2 value of 0.60 ± 0.34 kcal/mol, and the E62D/E84D double variant yielded a ΔG_{1+2} value of 1.47 ± 0.74 kcal/mol. The $\Delta\Delta G_B$ (k_{cat}) value, defined as $\Delta\Delta G_B = \Delta G_{1+2} - \Delta G_1 - \Delta G_2$, was 0.15 ± 1.41 kcal/mol. A similar analysis was applied to the k_{cat}/K_m values for these same variants, yielding a $\Delta\Delta G_B$ (k_{cat}/K_m) value of -0.33 ± 3.22 kcal/mol.

The k_{cat} value of the E62A/E84A double variant increased by 140% (2.4-fold) in imidazole versus that in MOPS buffer, while the E62A/E84A k_{cat}/K_m value increased by 4.8% in imidazole versus that in MOPS buffer (Supporting Information). This slight degree of imidazole rescue is similar to that observed for the single E62A variant. The k_{cat} value of the E62D/E84D double variant decreased 9.1% in imidazole versus that in MOPS buffer, while the E62D/E84D k_{cat}/K_m value decreased 52% in imidazole versus that in MOPS buffer (Supporting Information). Similar kinetic inhibition of both k_{cat} and k_{cat}/K_m by imidazole was observed for the single E62D variant.

DISCUSSION

Residues adjacent to the active site zinc in Cam, the prototype of an independently evolved γ-class of carbonic anhydrase, bear no resemblance to residues in the well-characterized α-class carbonic anhydrase II for which catalytic functions have been assigned (*1*, *22*). The high-resolution crystal structures of the zinc and cobalt forms of Cam complexed with bicarbonate provide a more detailed understanding of the active site and identify residues for which functions were proposed (*27*). Here, we describe the first site-specific replacement studies for Cam that test the proposed functions for active site residues.

Glu 84 Functions as a PSR. Cam exhibits a k_{cat} approaching 10^5 s^{-1} for the CO_2 hydration reaction, implying the presence of an ionizable residue in the vicinity of the Cam active site that functions as a PSR. Three lines of evidence presented here establish that Glu 84 is a PSR in Cam. First, only the replacement of Glu 84 with ionizable residues capable of proton transfer (histidine and aspartate) and with intrinsic pK_a values near that of glutamate produced variants with robust k_{cat} values relative to that of the wild type when assayed in the bulky buffer MOPS. Except for E84Y, the Glu 84 variants exhibited only moderate changes in k_{cat}/K_m relative to that of the wild type, indicating that Glu 84 has a minimal role in the CO_2 hydration step of catalysis (eq 2). In addition to an intrinsic pK_a of 10 which makes tyrosine a poor PSR at pH 7.5, the large aromatic side chain may sterically hinder substrate binding or product release. Second, the k_{cat} values of the E84A, -C, -K, -Q, -S, and -Y variants were increased up to 46-fold by replacement of MOPS with imidazole buffer, regardless of side chain size and shape, reminiscent of imidazole rescue reported for the PSR H64A variant of the α-class carbonic anhydrase II (*3*, *4*). Imidazole rescue also provides additional support that replacements of Glu 84 did not produce global conformational changes leading to the low k_{cat} values relative to that of the wild type. A simple interpretation of these results is that imidazole enters the active site of the Glu 84 variants and transfers a proton directly between the metal-bound water molecule and bulk solvent, thereby replacing the PSR function of Glu 84. The imidazole-dependent inhibition of k_{cat}/K_m for the wild type and the E84A variant implies that imidazole enters the active site and binds near the site of CO_2 hydration, presumably to zinc (*33*, *34*). MOPS is unable to mimic imidazole, apparently as a consequence of its larger size and inability to enter the active site. Third, there was a marked deviation in the pH versus k_{cat} profile for the E84H variant compared to that of the wild type, although the k_{cat} values were robust relative to the wild-type value. These results suggest that histidine in position 84 is functioning as a PSR similar to Glu 84.

There are several possible reasons for the failure of acetate to rescue the E84A variant. First, acetate significantly inhibits the CO_2 hydration rate of wild-type Cam (Table 1). This inhibition may be similar to that observed for α-class carbonic anhydrases in which one oxygen of the acetate carboxylate group binds directly to the zinc ion (*35*). Thus, any acetate rescue of E84A may be overwhelmed by decreases in the rate of ionization of the zinc-bound water molecule, or attack of the resultant hydroxide ion on bound CO_2, due to steric blocking of the zinc ion by a bound acetate molecule. Second, acetate has a much lower intrinsic pK_a of 4.7 than imidazole (pK_a = 7.0), and is mainly in its ionized state at pH 7.5. Thus, acetate may be too weak as a proton acceptor at pH 7.5 and unable to replace the function of the Glu 84 PSR which may have a higher pK_a value of 6−7 when covalently positioned between acidic residues Glu 62 and Glu 88. The failure of acetate and the success of imidazole in rescuing the E84A variant are consistent with this proposal, and the proposal that the decreased k_{cat} value and pH dependence of k_{cat} for the E84H variant (relative to that of the wild type) is a consequence of a lowered pK_a for

histidine when incorporated at this position.

Previous studies (*26*) identified two pK_a values (pK_a^I = 6.7−6.9, pK_a^{II} = 8.2−8.4) in the profile of k_{cat}/K_m versus pH of wild-type Cam. It was proposed that pK_a^I reflects ionization of the zinc-bound water molecule. The identity of the second ionizable group responsible for pK_a^{II} is unresolved. The two nearly identical pK_a^I values of 6.5 and 6.6 observed for the wild type and the E84H variant indicate that this ionization is not significantly affected by the substitution, a result consistent with the previous proposal that pK_a^I reflects ionization of the zinc-bound water (*26*). Although the pK_a^{II} for wild-type Cam (8.5) reported here is in agreement with the previously published value of 8.2−8.4 (*26*), the pH profile for the E84H variant k_{cat}/K_m value yields a fit pK_a^{II} value of 9.7. This increase in pK_a^{II} indicates that the ionization state of either glutamate or histidine in position 84 indirectly influences the CO_2 hydration step in catalysis. This conclusion for Cam has precedent in α-class carbonic anhydrases. Substitution of Tyr 64 with histidine in carbonic anhydrase V allows histidine to function as a PSR and induces a second pK_a in the profile of k_{cat}/K_m versus pH (*8*). Furthermore, the k_{cat}/K_m versus pH profile for esterase activity of carbonic anhydrase II reveals a second pK_a attributed to His 64 (*36*). The mechanism by which substitution of histidine at position 84, 8 Å removed from the active site zinc, perturbs pK_a^{II} in Cam is unknown. Histidine could potentially influence the pK_a of the adjacent Glu 62 residue for which the results presented here establish a role in the CO_2 hydration step of catalysis (eq 2).

Glu 62 Is Important for the CO_2 Hydration Step in Catalysis, but Its Function as a PSR Is Unresolved. In high-resolution crystal structures of Cam (*27*), bicarbonate is ligated to the metal ion and also hydrogen bonds with Glu 62, leading to the proposal that this residue functions in the CO_2 hydration step of catalysis (eq 2) to stabilize the transition state. Only the E62D variant had robust k_{cat} and k_{cat}/K_m values relative to that of the wild type, suggesting a carboxyl group in this position is important for optimum function and that the active site is partially able to adapt to displacement of the carboxyl group by one methylene carbon. All other variants had low k_{cat} and k_{cat}/K_m values relative to that of the wild type, indicating perturbation of the CO_2 hydration step (eq 2). The low k_{cat} value observed for the isosteric E62Q variant indicates that Glu 62 does not simply provide a space-filling function in the Cam active site. These results indicate that Glu 62 is important for the CO_2 hydration step (eq 2) of catalysis. The higher k_{cat}/K_m values for the E62C, E62Q, and E62T variants in MOPS buffer compared with that of the E62A variant are consistent with the proposed hydrogen bonding function for Glu 62 in stabilization of metal-bound bicarbonate during catalysis (*27*). The side chains of glutamine, threonine, and cysteine can function as hydrogen bond donors and acceptors potentially fulfilling the proposed role for Glu 62, although not as efficiently as glutamate. Although histidine and tyrosine are also potential hydrogen bond donors and acceptors, the k_{cat} values for the E62H and E62Y variants were significantly lower than those for E62C, E62Q, and E62T and may be a consequence of the more bulky side chains of histidine and tyrosine that sterically hinder the active site.

It is also postulated that Glu 62 is important in the proton transfer step of catalysis and shuttles protons between zinc-bound water and Glu 84, on the basis of recent high-resolution crystal structures (*27*). Both k_{cat} and k_{cat}/K_m values of the Glu 62 variants were low relative to the wild-type value; thus, it was not possible to conclude that this residue also functions as a PSR. Although histidine could potentially replace the proposed PSR function of Glu 62, the k_{cat} value of E62H was only 2% of the wild-type value; however, it is also possible that the CO_2 hydration step is rate-limiting for this variant, thereby masking a surrogate proton transfer function for histidine at position 62. Likewise, it is possible that the inability of imidazole to enhance k_{cat} more than 4-fold for any of the Glu 62 variants, or either of the E62A/E84A and E62D/E84D double variants, is a result of the CO_2 hydration step becoming rate-limiting. A rate-limiting CO_2 hydration step is only one of several possibilities that might explain these negative results; thus, it was not possible to determine if Glu 62 is also important for the proton transport step in catalysis. Nonetheless, several observations are consistent with this role for Glu 62. First, Glu 84 is established as a PSR and is at least 8 Å away from the active site zinc, indicating a requirement for intervening molecules to transfer protons from the zinc-bound water to Glu 84. Glu 62 is positioned between the active site zinc and one of the three Glu 84 side chain conformers in the high-resolution crystal structure of Cam (*27*). Second, kinetic and thermodynamic analyses of single and double variants suggest Glu 62 and Glu 84 interact during catalysis. The decrease in the k_{cat} value of the double variant E62D/E84D relative to the wild-type value was greater than for either of the single E62D and E84D variants. Single substitutions may be offset by the conformational flexibility of the enzyme backbone structure or re-ordering of nearby solvent molecules, while the double substitution may result in side chains that are too short for the carboxylate groups to interact effectively for proton transfer. In addition to the kinetic analyses, the positive value for $\Delta\Delta G_B$ (k_{cat}) indicates that residues Glu 62 and Glu 84 interact either in a slightly synergistic manner or possibly in an additive manner during proton transfer. The negative value obtained for $\Delta\Delta G_B$ (k_{cat}/K_m) indicates a slightly antagonistic interaction between Glu 62 and Glu 84 during the CO_2 hydration step of catalysis. However, the large errors inherent in these calculations leave room for other interpretations, including no interaction, or antagonistic, synergistic, or additive interactions between Glu 62 and Glu 84 during both the CO_2 hydration (eq 2) and proton transfer steps (eq 3) of catalysis. An alternate proton transport pathway is also possible in which protons are transferred from the active site zinc to Glu 84 by a network of hydrogen-bonded water molecules. In this mechanism, the Glu 62 side chain carboxylate group may orient or polarize adjacent water molecules involved in proton transport, rather than directly transferring protons.

Glu 88 and Glu 89 Have a Minor Role in the Proton Transfer Step of Catalysis. Only a 2-fold decrease in k_{cat} relative to the wild-type value for the E88A and E89A variants suggests that these external loop residues are only of minor importance for catalysis. Only the k_{cat} value of the variants decreased relative to that of the wild type, which suggests these residues are involved in the proton transport step and not the CO_2 hydration step of catalysis. The small 2-fold imidazole rescue of k_{cat} for the E88A and E89A variants is not unexpected considering the small decrease in

k_{cat} for these variants compared to that of the wild type; thus, these results do not rule out a proton transfer function for these residues. Other observations are consistent with a PSR function. In one of the Glu 84 conformations (*27*), its side chain is pointed toward Glu 88, suggesting an interaction between these residues. It is possible that Glu 88 and Glu 89 may interact with each other to further relay protons between Glu 84 and buffer molecules through a proton wire. However, there may be different mechanisms for transferring protons from Glu 84 to buffer, explaining why the E88A and E89A variants exhibit a less than 2-fold decrease in k_{cat} relative to the wild-type value. Clearly, other external Cam residues should be investigated with regard to their role in proton transport.

Comparison between Cam and α-Class Carbonic Anhydrases. Although Cam clearly evolved independently of the α-class carbonic anhydrases, some aspects of the mechanism of Cam appear to be analogous to that of the fast carbonic anhydrases of the α-class. Both Cam and the α-class structures contain an active site zinc ion coordinated by three histidines with very similar side chain orientations; both types of enzymes also use similar zinc hydroxide mechanisms in the CO_2 hydration reaction (*1*, *22*, *26*). Cam and fast α-class enzymes also use PSRs to assist in removal of protons generated by ionization of zinc-bound water. In Cam, the primary PSR is residue Glu 84, while in the α-class carbonic anhydrase II enzyme, the primary PSR is residue His 64. There are a number of structural and functional similarities between these two PSRs. First, substitutions of Cam Glu 84 result in functional variants when other ionizable residues such as aspartate and histidine replace Glu 84. Similar allowed ionizable residue substitutions are observed for position 64 residue in α-class carbonic anhydrase II, III, and V enzymes (*4*, *8*, *9*, *37*). Second, both Cam E84A and α-class carbonic anhydrase II H64A variants exhibit low k_{cat} values that are rescued by small imidazole buffers (*3*, *38*) and concentration-dependent inhibition of k_{cat}/K_m values by imidazole (*3*). Third, the corresponding distances between the Cam Glu 84 PSR α-carbon and active site zinc (8 Å) and the α-class carbonic anhydrase II His 64 PSR α-carbon and its respective active site zinc (10 Å) are similar. Distances between the respective Glu 84 and His 64 side chain proton donor and/or acceptor groups (Glu 84 carboxylate oxygen, His 64 imidazole, and ϵ-2 nitrogen) and active site zinc ions are also very similar, 8 Å for both enzymes, in some of the observed side chain conformations. A fourth structural similarity between the Cam Glu 84 PSR and the α-class carbonic anhydrase II His 64 PSR is that multiple side chain conformations have been observed for both of these residues in crystal structures. Two side chain conformations were observed for the His 64 PSR in α-class carbonic anhydrase II (*39*−*41*), dependent on the protonation state of the imidazole side chain. Recent high-resolution crystal structures of Cam (*27*) reveal three distinct conformations for the Glu 84 side chain.

Although the Glu 62 residue was shown to be important for catalysis in Cam, the active site of the α-class carbonic anhydrase II enzyme does not have an equivalent acidic ionizable glutamate or aspartate residue exposed in the active site near the zinc ion. However, carbonic anhydrase II has a Thr 199 residue that is polarized (hydrogen-bonded) by the adjacent Glu 106 residue (*1*). In addition to orientation of the lone pair of electrons on the zinc-bound hydroxyl for nucleophilic attack on CO_2, it is proposed that Thr 199 also has a "door-keeper" function in selecting only protonated molecules to bind to the active site (*1*). Thus, Glu 62 may have a door-keeper role analogous to that of the Thr 199 and Glu 106 pair in the α-class carbonic anhydrases as suggested by recent high-resolution crystal structures of Cam in which Glu 62 also binds the bicarbonate product (*27*). These recent crystal structures of Cam (*27*) suggest other active site residues (Gln 75 and Asn 202) may fulfill catalytic roles analogous to the other functions assigned to Thr 199 of the α-class carbonic anhydrases.

Although residues in the active site of Cam may have functions analogous to those of residues essential for catalysis in the active site of the α-class enzymes, the mechanisms of Cam and the α-class may have significant differences. On the basis of the recent crystal structure for a β-class carbonic anhydrase, it was suggested that the mechanism of the α- and β-class enzymes are similar but distinct from the γ-class (*42*)**.** The SHIE on the k_{cat}/K_m values of α-class enzymes are close to unity (*43*), while a moderate SHIE of 1.6−1.8 was observed in the k_{cat}/K_m value of Cam over the pH range of 6.5−8.5. This result indicates that the CO_2 hydration step (eq 2) of Cam also contains a rate-contributing proton transfer event or that a significant change occurs in the hydrogen-bonded network of active site molecules during the catalytic step described by the parameter k_{cat}/K_m (eq 2). Thus, Cam may have a somewhat different catalytic mechanism for the CO_2 hydration step (eq 2) than that accepted for the α- and β-class carbonic anhydrases. There are other well-characterized zinc enzymes with unrelated tertiary structures that have active site structures similar to Cam. Bovine pancreatic carboxypeptidase A is one example that has a solvent-accessible glutamate residue (Glu 270) that is important for catalysis located in the active site (*44*, *45*). In this enzyme, the Glu 270 carboxylate oxygens are located 4.5−5.3 Å from the active site zinc ion (*46*−*48*). In the proposed "promoted-water" mechanism, ionization of a zinc-bound water molecule is assisted by the Glu 270 residue functioning as a general base (*44*). The resulting zinc-bound hydroxide ion then attacks the peptide bond. Thermolysin is another example of a zinc metalloenzyme that contains an important catalytic glutamate residue in the active site. In this enzyme, a Glu 143 residue is located in the active site with its carboxylate oxygens 4.4−5.2 Å from the zinc ion (*49*, *50*). This enzyme is thought to function via a zinc hydroxide mechanism with the Glu 143 acting as a general base to extract a proton from a zinc-bound water molecule (*51*). Thus, it is likely that the Glu 62 residue in Cam functions in a similar manner, assisting in ionization of the zinc-bound water molecule, prior to hydroxide attack on the bound CO_2 molecule, as suggested by Iverson et al. (*27*). Cocrystal structures of Cam with bicarbonate also indicate a role for Glu 62 in stabilizing the transition state and binding and release of the bicarbonate product (*27*). The proposed multiple roles of Glu 62 in both steps of catalysis (eqs 2 and eq 3) may explain the observed nonunity SHIE on both k_{cat} and k_{cat}/K_m values of the wild type. The lowered k_{cat} and k_{cat}/K_m values and the decreased SHIE on k_{cat} at pH 6.5 observed for wild-type Cam (Table 2) may result from a decreased ability of the Glu 62 residue to ionize and participate in catalysis by abstracting and/or transferring

protons at lower pH values. It is also possible that the SHIE on both k_{cat} and k_{cat}/K_m results from participation of other active site polar residues in hydrogen bonding or proton transfer during the CO_2 hydration step of catalysis (eq 2), such as Gln 75.

ACKNOWLEDGMENT

We thank David Silverman, Chingkuang Tu, Carol Fierke, Teaster T. Baird, C. Robert Matthews, Brandon Doyle, and Kerry Smith for many helpful discussions and technical assistance.

SUPPORTING INFORMATION AVAILABLE

Additional steady-state Michaelis−Menten kinetic parameter data for the E62C, -D, -H, -Q, -T, and -Y, E84C, -D, -H, -K, -Q, -S, and -Y, E62A/E84A, E62D/E84D, E88A, and E89A Cam variants in pH 7.5, 50 mM imidazole buffer, for the wild type and E62A and E84A Cam variants in pH 7.5, 50 mM MOPS, 50 mM pyrazole buffer, and for the E84A Cam variant in pH 7.5, 50 mM 1-methylimidazole and pH 7.5, 1,2-dimethylimidazole buffer, where all the assays were performed with the ionic strength adjusted to 0.2 M with Na_2SO_4. This material is available free of charge via the Internet at http://pubs.acs.org.

REFERENCES

1. Lindskog, S. (1997) *Pharmacol. Ther. 74*, 1−20.
2. Lindskog, S., and Coleman, J. E. (1973) *Proc. Natl. Acad. Sci. U.S.A. 70*, 2505−2508.
3. Tu, C. K., Silverman, D. N., Forsman, C., Jonsson, B. H., and Lindskog, S. (1989) *Biochemistry 28*, 7913−7918.
4. Engstrand, C., Forsman, C., Liang, Z., and Lindskog, S. (1992) *Biochim. Biophys. Acta 1122*, 321−326.
5. Silverman, D. N., Tu, C., Chen, X., Tanhauser, S. M., Kresge, A. J., and Laipis, P. J. (1993) *Biochemistry 32*, 10757−10762.
6. Liang, Z., Jonsson, B.-H., and Lindskog, S. (1993) *Biochim. Biophys. Acta 1203*, 142−146.
7. Taoka, S., Tu, C., Kistler, K. A., and Silverman, D. N. (1994) *J. Biol. Chem. 269*, 17988−17992.
8. Heck, R. W., Boriack-Sjodin, P. A., Qian, M., Tu, C., Christianson, D. W., Laipis, P. J., and Silverman, D. N. (1996) *Biochemistry 35*, 11605−11611.
9. Qian, M., Tu, C., Earnhardt, J. N., Laipis, P. J., and Silverman, D. N. (1997) *Biochemistry 36*, 15758−15764.
10. Hurt, J. D., Tu, C., Laipis, P. J., and Silverman, D. N. (1997) *J. Biol. Chem. 272*, 13512−13518.
11. Earnhardt, J. N., Qian, M., Tu, C., Laipis, P. J., and Silverman, D. N. (1998) *Biochemistry 37*, 7649−7655.
12. Earnhardt, J. N., Qian, M., Tu, C., Lakkis, M. M., Bergenhem, N. C., Laipis, P. J., Tashian, R. E., and Silverman, D. N. (1998) *Biochemistry 37*, 10837−10845.
13. Tu, C., Qian, M., Earnhardt, J. N., Laipis, P. J., and Silverman, D. N. (1998) *Biophys. J. 74*, 3182−3189.
14. Qian, M., Earnhardt, J. N., Wadhwa, N. R., Tu, C., Laipis, P. J., and Silverman, D. N. (1999) *Biochim. Biophys. Acta 1434*, 1−5.
15. Earnhardt, J. N., Wright, S. K., Qian, M., Tu, C., Laipis, P. J., Viola, R. E., and Silverman, D. N. (1999) *Arch. Biochem. Biophys. 361*, 264−270.
16. Venkatasubban, K. S., and Silverman, D. N. (1980) *Biochemistry 19*, 4984−4989.
17. Eriksson, A. E., Jones, T. A., and Liljas, A. (1988) *Proteins: Struct., Funct., Genet. 4*, 274−282.
18. Merz, K. M., Hoffmann, R., and Dewar, M. J. S. (1989) *J. Am. Chem. Soc. 111*, 5636−5649.
19. Håkansson, K., Carlsson, M., Svensson, L. A., and Liljas, A. (1992) *J. Mol. Biol. 227*, 1192−1204.
20. Jackman, J. E., Merz, K. M., and Fierke, C. A. (1996) *Biochemistry 35*, 16421−16428.
21. Lu, D., and Voth, G. A. (1998) *Proteins: Struct., Funct., Genet. 33*, 119−134.
22. Silverman, D. N. (1991) *Can. J. Bot. 69*, 1070−1078.
23. Smith, K. S., and Ferry, J. G. (1999) *J. Bacteriol. 181*, 6247−6253.
24. Bjorkbacka, H., Johansson, I. M., and Forsman, C. (1999) *Arch. Biochem. Biophys. 361*, 17−24.
25. Kisker, C., Schindelin, H., Alber, B. E., Ferry, J. G., and Rees, D. C. (1996) *EMBO J. 15*, 2323−2330.
26. Alber, B. E., Colangelo, C. M., Dong, J., Stalhandske, C. M., Baird, T. T., Tu, C., Fierke, C. A., Silverman, D. N., Scott, R. A., and Ferry, J. G. (1999) *Biochemistry 38*, 13119−13128.
27. Iverson, T. M., Alber, B. E., Kisker, C., Ferry, J. G., and Rees, D. C. (2000) *Biochemistry 39*, 9222−9231.
28. Alber, B. E., and Ferry, J. G. (1996) *J. Bacteriol. 178*, 3270−3274.
29. Sambrook, J., Fritsch, E. F., and Maniatis, T. (1989) *Molecular Cloning: A Laboratory Manual*, Cold Spring Harbor Laboratory Press, Cold Spring Harbor, NY.
30. Khalifah, R. G. (1971) *J. Biol. Chem. 246*, 2561−2573.
31. Honig, B., and Nicholls, A. (1995) *Science 268*, 1144−1149.
32. Mildvan, A. S., Weber, D. J., and Kuliopulos, A. (1992) *Arch. Biochem. Biophys. 294*, 327−340.
33. Kannan, K. K., Petef, M., Fridborg, K., Cid-Dresdner, H., and Lovgren, S. (1977) *FEBS Lett. 73*, 115−119.
34. Khalifah, R. G., Zhang, F., Parr, J. S., and Rowe, E. S. (1993) *Biochemistry 32*, 3058−3066.
35. Håkansson, K., Briand, C., Zaitsev, V., Xue, Y., and Liljas, A. (1994) *Acta Crystallogr. D50*, 101−104.
36. Simonsson, I., and Lindskog, S. (1982) *Eur. J. Biochem. 123*, 29−36.
37. Tu, C., Chen, X., Ren, X., LoGrasso, P. V., Jewell, D. A., Laipis, P. J., and Silverman, D. N. (1994) *J. Biol. Chem. 269*, 23002−23006.
38. Forsman, C., Behravan, G., Jonsson, B.-H., Liang, Z., Lindskog, S., Ren, X., Sandstrom, J., and Wallgren, K. (1988) *FEBS Lett. 229*, 360−362.
39. Krebs, J. F., Fierke, C. A., Alexander, R. S., and Christianson, D. W. (1991) *Biochemistry 30*, 9153−9160.
40. Nair, S. K., and Christianson, D. W. (1991) *J. Am. Chem. Soc. 113*, 9455−9458.
41. Nair, S. K., and Christianson, D. W. (1991) *Biochem. Biophys. Res. Commun. 181*, 579−584.
42. Kimber, M. S., and Pai, E. F. (2000) *EMBO J. 19*, 1407−1418.
43. Steiner, H., Jonsson, B. H., and Lindskog, S. (1975) *Eur. J. Biochem. 59*, 253−259.
44. Christianson, D. W., and Lipscomb, W. N. (1989) *Acc. Chem. Res. 22*, 62−69.
45. Vendrell, J., and Aviles, F. X. (1999) in *Proteases: new perspectives* (Turk, V., Ed.) pp 13−34, Birkhauser Verlag, Basel, Switzerland.
46. Bukrinsky, J. T., Bjerrum, M. J., and Kadziola, A. (1998) *Biochemistry 37*, 16555−16564.
47. Massova, I., Martin, P., deMel, S., Tanaka, Y., Edwards, B., and Mobashery, S. (1996) *J. Am. Chem. Soc. 118*, 12479−12480.
48. Greenblatt, H. M., Feinberg, H., Tucker, P. A., and Shoham, G. (1998) *Acta Crystallogr. D54*, 289−305.
49. Holmes, M. A., and Matthews, B. W. (1982) *J. Mol. Biol. 160*, 623−639.
50. Holland, D. R., Hausrath, A. C., Juers, D., and Matthews, B. W. (1995) *Protein Sci. 4*, 1955−1965.
51. Matthews, B. W. (1988) *Acc. Chem. Res. 21*, 333−340.

BI0001877